IET Power Electronics

WILEY

The Institution of Engineering and Technology

ORIGINAL RESEARCH OPEN ACCESS

Pareto-Based Design Optimisation of Hybrid Energy Storage Systems for Full-Electric Vessels

Rene A. Barrera-Cardenas[1] | Salvatore D'Arco[1] | Luigi Piegari[2] | Pietro Tricoli[3]

[1]Energy Systems Department, SINTEF Energy Research, Trondheim, Norway | [2]Politecnico di Milano, DEIB – Politecnico di Milano, Milano, Italy | [3]Electronic, Electrical and Systems Engineering, University of Birmingham, Birmingham, UK

Correspondence: Rene A. Barrera-Cardenas (rene.barrera-cardenas@sintef.no)

Received: 7 November 2024 | **Revised:** 17 February 2025 | **Accepted:** 18 March 2025

Funding: This research was supported by the Horizon Europe Program 101096831.

ABSTRACT

Full electric vessels can benefit from hybrid energy storage systems (HESS) that combine two storage technologies of different characteristics in terms of power and energy density. The optimal design of a HESS for a vessel is generally a rather complex multivariable optimization with several degrees of freedom and constraints. Indeed, the optimization should account for the operational characteristics of the storage units, including their progressive aging. Moreover, the sizing of the storage units is tightly linked to the strategy implemented in the energy management system (EMS) for allocating the power needed by the load to the storage units. This paper presents a two-stage Pareto-based design optimization procedure for HESS intended for a full-electric vessel. The methodology first identifies a Pareto front as the set of all the optimal configurations in terms of capacity of the two storage units that fulfil the operational constraints within a large discrete configuration space. These constraints account for capacity degradation and limitations in power and energy. The degrees of freedom in the EMS are included in the configuration space. A second stage identifies the optimal configuration on the Pareto front based on a defined cost function. The approach decouples the analysis of the solutions that can fulfil the operational constraints from the optimization and can be very effective in exploring the effect of several alternative cost functions on the optimal solution. Moreover, the shape of the Pareto front can offer a visual clue to the benefits offered by a hybrid storage compared to a single technology solution and on the optimization margins. The procedure is illustrated with a case of a full electric tugboat highlighting when a HESS can be beneficial and how the optimal design can be facilitated.

1 | Introduction

Energy storage systems (ESSs) are widely used to compensate for imbalances between power generation and power demand in electrical systems, especially when the regulation of the generated power or of power demand is not feasible or convenient. The selection of the most appropriate storage technology and the design of the ESS are critical to ensure technically and economically efficient operations. This is normally achieved by matching the energy and power densities of the ESS to the application requirements. In marine applications, the operational power demand profiles present a very large degree of variability even within a single category of vessels, due to the possibility of the occurrence of unusual environmental conditions, emergency operation needs, or specific service requirements [1]. When a single type of storage technology is selected to address all application requirements and environmental conditions, the designed power and energy of the ESS may be significantly larger than the value required to fulfil the basic operational requirements, leading to a high-cost storage system. One solution to mitigate this issue is to define energy management strategies that actively regulate the power demand to optimise the efficiency and lifetime of the ESS by considering its operational constraints [2]. An alternative option is represented by hybrid ESSs (HESSs) combining two storage technologies [3, 4] with complementary characteristics in terms of power and energy densities. Thus, a HESS will contain a high-energy (HE) ESS and high-power (HP) ESS. The optimal design of a HESS for a vessel, accounting for all the operational requirements, can be challenging due to the many degrees of freedom and constraints. The design of HESSs has been extensively addressed in the technical literature for a wide range of applications and use cases. This is clearly demonstrated by the large number of review papers on the topic [5–14]. A discriminating element is the availability of an external source acting as a slack node. This occurs in stationary applications where the grid acts as the slack node, allowing for lower constraints on the power and energy of the HESS [7, 9, 12]. On the contrary, the lack of a slack node, as in fully electric vessels, leads to strict power and energy requirements for HESSs that need to be specifically reflected in their sizing process. The lack of a slack node is common in all traction applications. Indeed, many papers propose sizing criteria and control strategies for HESS in electric vehicles, as discussed in the following review papers [6, 8, 10, 11, 13, 14]. It is worth noting that electric marine applications are a very recent topic addressed in the technical literature. Indeed, in [15], the authors claim to be the first to investigate the optimal sizing and cost assessment of the hybrid battery system based on the integration of HE and HP Li-ion cells for marine applications. Although the application of HESS in marine environments shares some similarities with their use in electric vehicles, there are significant differences due to distinct operational constraints. First, marine vessels require considerably higher power levels than electric vehicles. As a result, certain solutions that are effective in one domain may not be as advantageous in the other. Moreover, while weight is a critical constraint for electric vehicles, it is less significant for marine vessels. Consequently, in the marine sector, power converters used to couple the two energy storage systems in a HESS are not as constrained by weight and size considerations. Given the lower power and energy requirements of electric vehicles, optimizing the weight and volume of power converters is crucial. In contrast, for marine applications, semi-active HESS configurations, which are commonly proposed for electric vehicles, are less promising due to the relatively negligible impact of power converter weight and size compared to that of the storage units. Moreover, in marine applications, energy storage units must undergo a marinization process, which can significantly alter their performance compared to other applications. For instance, due to safety requirements and mechanical stresses, battery enclosures must be considerably larger than those used in electric vehicle applications. This results in a reduction in both energy and power density, making marine batteries inherently less compact and efficient in terms of volumetric and gravimetric performance.

The allocation of the energy demand between individual storage devices of the HESS is a critical aspect, and several optimal control strategies have been proposed for electric vehicles [16, 17]. Indeed, the strategies for power allocation and the design criteria for sizing the storage devices in a HESS are tightly linked, and both should be accounted for in a design optimisation, but this is not sufficiently considered in several papers focusing on marine applications. An optimal design of an ESS based on a single storage technology for marine applications, considering the effect of the power profile and ageing has been proposed in [18, 19], but the results are not easily extendable to a HESS because the allocation of the power between the storage devices is not addressed. An integrated design procedure to optimise a HESS considering the energy management strategy has been proposed by Trovão et al. in [4], but it is based on a passive hybridisation system where supercapacitors (SC) and lithium-ion batteries (LiB) are directly paralleled without any power electronic interface. Therefore, the power allocation between the HE-ESS and HP-ESS is not controllable. In [20], Kim et al. introduced a hybrid power system for bulk carriers, combining conventional diesel generators with a battery/supercapacitor HESS for port operations. LiBs act as HE-ESS for vessel manoeuvring in port, while SC act as HP-ESS for crane operation when the vessel is moored. Albeit the paper has demonstrated improved efficiency, reduced emissions, and savings for bulk carriers, the potential synergies between the two storage technologies have not been exploited because the two ESSs are used separately.

Balsamo et al. addressed in [21] the optimal design and energy management of a HESS for fully electric boats in inland waterways, proposing a methodology to evaluate the design, maintenance, and cost of marine transport systems. The proposed procedure calculates the capacity of LiBs and SCs, and the control rules of the energy management system (EMS) to assign the power profiles to the two storage units with the objective of minimising the battery current. The optimal solution aims at improving the lifetime and the efficiency of the HE-ESS, assuming that the ageing, losses and energy contribution of the HP-ESS are negligible. While this proposal can be effective when ESS characteristics are very different, as for lead-acid batteries and SC, its effectiveness and applicability are rather limited for storage devices with more similar characteristics, such as LiBs with different chemistries. Therefore, the results cannot be applied in more modern vessels in which the use of lithium batteries will substitute the lead-acid technology. The possibility of using LiBs with different chemistries for usage as HE-ESS and HP-ESS was studied in [15]. In this paper, a reference load cycle is selected for the vessel, and the HE-ESS supplies preferentially the load power up to its maximum power. If the load power exceeds this value, the difference is covered by the HP-ESS. This rule-based design defines univocally the power profiles for the two ESSs and allows the calculation of their minimum size and cost to ensure at least ten years of operation. While this procedure is applicable for different types of energy storage devices and EMS, the recharge phase of the energy storage is not addressed, and can alter significantly the results. Indeed, with partial recharge of the HP-ESS, it is possible to implement peak-shaving features that result of improvements of the overall system efficiency. Moreover, only the total cost of the storage is considered as a quantity to minimize, while other important aspects, like the overall volume and the efficiency of the HESS, are not considered.

In [22], Forestieri et al. used a deep reinforcement learning method to design, at the same time, the sizes of LiBs and of SCs in a HESS by selecting the most appropriate frequency of a low-pass filter for the EMS to allocate the power between the two storage units. The proposed method is independent of the knowledge of the load profile and can be implemented in real time. The objective function to be minimised is defined considering the battery current limit, power losses, overall cost, with the additional condition that the initial and final state of charge of the storage devices are at the same level. Even if this procedure is effective, the sensitivity of the different constraints is not easily understandable, and it is difficult to assess how much the solution is affected by the weight values. Moreover, the total energy and volume of the HESS are not considered, albeit they are the most important parameters for a vessel. In [23], Tao et al. proposed a HESS design for full-electric marine applications for the combination of HE and HP batteries. A low-pass filter is used as power-split algorithm between HE-ESS and HP-ESS, while restricting the energy transfer between HE batteries and HP batteries, which reduces the cycled energy from HE-ESS but also may end up in overestimation of the required energy for HP-ESS if multiple discharge cycles should be delivered before charging power is available. Moreover, battery aging is simplified and does not consider current rates and temperature dependencies, while multiple studies [24–26] demonstrated these are strongly affecting battery degradation.

The optimal design of a HESS for a vessel is generally a rather complex multivariable optimization with several degrees of freedom and constraints that should be appropriately accounted for to achieve reliable results. Indeed, the optimization should consider the operational characteristics of the storage units, including their progressive aging. Moreover, the sizing of the storage units is tightly linked to the strategy implemented in the EMS for allocating the power needed by the load to the storage units. The goal of a HESS design methodology is to identify the optimal sizing (i.e., minimum capacity to be installed) for each storage device. However, the presence of multiple constraints and degrees of freedom with conflicting effects on the required capacity of each storage unit is a challenging aspect of the optimisation procedure. The papers available in the technical literature search for an optimal sizing based on an objective function to minimize. Even if this allows identifying an optimal solution, the whole optimization process must be repeated if the objective function changes. Moreover, it is difficult to capture the sensitivity of the optimal configuration based on the specific choice of the cost function. This is especially relevant when the parameters in the cost function may be affected by uncertainties, and the robustness of the optimal solution is a relevant aspect to consider. The concept of Pareto optimality is at the foundation of several approaches for solving multi-objective optimization problems having conflicting objectives [27] but has not been applied yet to the optimal sizing of a HESS for marine applications. Instead of identifying individual solutions, a large set of Pareto optimal solutions is generated forming the Pareto front. The assessment of the optimal solutions with regard to a defined cost function can be restricted to the evaluation of the configurations lying on the Pareto front avoiding to repeatedly explore the entire configuration space domain.

This paper is the first to apply a Pareto-based optimization to the optimal sizing of a hybrid energy storage for a fully electric vessel. The approach consists of two main stages. First, the Pareto front is identified as the set of all the optimal configurations in terms of minimum required installed capacities of HE-ESS and HP-ESS for the HESS that fulfil the operational constraints within a very large discrete design space. The considered HESS topology includes two storage technologies with fully controllable power flows via power converters. The operational constraints account for capacity degradation and limitations in power and energy. A multi-factor degradation model [24, 19] is adopted that accounts for depth of discharge, current rates, and temperature dependencies to estimate the degradation per cycle, which improves the ESS degradation estimation, especially when short power pulses are contained in the main discharge cycle. The degrees of freedom in the configuration of the energy management system are also included in the configuration space. A saturated low-pass filter is assumed to split the power profiles of the HE-ESS and HP-ESS, whose effectiveness has been demonstrated in [22, 23, 28]. An additional degree of freedom is considered by incorporating and comparing three charging strategies for the HE-ESS and HP-ESS. This allows setting a higher priority on either the HE-ESS or HP-ESS power charge and usable energy, resulting in a better exploration of energy and power requirements for the HE-ESS and HP-ESS, compared with previous works. A second stage identifies the optimal configuration on the Pareto front based on a defined cost function. The approach decouples the analysis of the solutions that can fulfil the operational constraints from the optimization and can be very effective in exploring the effect of several alternative cost functions on the optimal solution. Moreover, the shape of the Pareto front can offer a visual clue about the benefits offered by hybrid storage compared to a single technology solution and a clear view of the optimization margins.

This paper describes this Pareto-based optimization and how to incorporate the degradation models and the energy management strategy into the process. Finally, a numerical example based on an electric tugboat is thoroughly illustrated to highlight, with a concrete example, the practical benefits of the approach presented. Batteries and supercapacitors are considered storage technologies. By exploring the different combinations of energy management strategy parameters and applying the ESS sizing algorithm to each split profile, the proposed Pareto-based design approach maps the main trade-offs between considered performance indicators (cost, volume, weight), producing a set of HESS design alternatives instead of a single solution, so the set of alternatives can be further analysed against size limitations onboard and market-available ESS configurations.

2 | Hybrid Storage Systems and Energy Pareto Optimality

The power and energy densities of storage technologies are the main discriminating characteristics for the selection of an ESS, because they are directly related to the capabilities to cover base loads for long intervals of time or short power peaks. In general, HE-ESS are characterized by lower power capabilities and limited cycling life compared to HP-ESS technologies. Li-ion batteries are the most popular HE and HP ESS for marine applications, while supercapacitors have been considered HP-ESS in a few applications. The main characteristics and performance of seven energy storage modules and systems, based on different chemistries/technologies, available for marine applications are presented in Table 1. Cells with graphite anode and nickel, manganese and cobalt cathode (G/NMC) show the highest energy density but the lowest specific power. Cells with graphite

TABLE 1 | Example of high-energy and high-power ESS modules/systems available for marine applications. (Values in parenthesis refers to full system performance).

Technology/chemistry	G/NMC-energy	G/LFP-energy	G/LFP-power	G/NMC-power	LTO/LMO	LTO/NMC	Super capacitor
Reference module (system)	XMP 123E [35] (XPAND XRS2)	Seanergy 48M (seanergy) [33]	Seanergy 48P (seanergy) [33]	Orca energy [46](orca energy)	24V70Ah G4.3 (Titan-IN) [32]	HP-7 [47](Pack)	SkelM162V62F (skelgrid) [38]
Manufacturer	Freudenberg ePS	Saft	Saft	Corvus energy	Altairnano	E-mobitech	Skeleton
Capacity [Ah]	138 (@ C/10)	80 (@ C/5)	60 (@ C/5)	128 (@ C/3)	68 (@ 1C)	10 (@ –)	2 (–)
Nominal energy [kWh]	12.3 (@ C/10)	3.7 (@ C/5)	2.6 (@ C/5)	5.65 (@ C/3)	1.5(@ 1C)	6.9 (@ –)	0.226 (@Vmax.)
Nominal voltage [V]	88.6	46.2	46.2	44.5	24	691	113
Voltage range [V]	64.8 – 97.9	37.8 – 53.2	37.8 – 53.2	36.4 – 50	17 – 27.5	519 – 800	64.8 – 162
Cell configuration	24s2p	14s2p	14s2p	13s3p	10s1p	290s1p[b]	54s1p
Cell type	Pouch	Cylindrical	Cylindrical	Pouch	Pouch	Pouch[b]	Cylindrical
Cooling method	Liquid	Forced air	Forced air	Forced air	Forced air	Liquid	Forced air
Module protection class	IP67	IP20	IP20	IP44	—	IP67	—
Discharge current rate [C-rate] (cont./peak[c])	1/2	2/3	4/6	3/5	7.4/13.3	20/36	124/380
Charge current rate [C-rate] (cont./peak[c]	0.4/0.5	1/2	4/6	3/5	7.4/13.3	20/36	124/380
Specific energy [Wh/kg]	160 (122)	96 (71)	69 (49)	94 (76)	53 (40)	– (26)	6.5 (4.1)
Energy density [Wh/dm3]	190 (110)	106 (92)	76 (63)	140 (87)	102 (44)	– (34)	5.9 (2.8)
Specific power [W/kg] (10s, 50%SoC)	259 (218)	281 (210)	396 (295)	380 (340)	700 (535)	– (920)	2450 (1560)
Power density [W/dm3] (10s, 50%SoC)	308 (242)	310 (273)	432 (385)	560 (389)	1350 (588)	– (1210)	2240 (1084)
Calendar life, 25°C @EOL (80%SOH)	20 years[a]	18 years	20 years	22 years[a]	25 years	25 years[a]	28 years[a]
Cycle life to 80%SOH.	4000 cycles @80%DoD, 0.3C/0.3C, 25°C	4000 cycles @80%DoD, 0.2C/0.2C, 25°C	6000 cycles @80%DoD, 0.8C/0.8C, 25°C	10,000 cycles[a] @80%DoD, 1.2C/1.2C, 30°C	25,000 cycles @100%DoD, 2C/2C, 25°C	60,000 cycles[b] @60%DoD, 5C/5C, 45°C	1,000,000 @75% DoD, 15C/15C, 35°C

[a]Assumed based on average calendar/cycling life of similar cell chemistries.

[b]Based on performance for 10Ah LTO cell from Toshiba [31].

[c]Peak for 10 s duration, continuous for at least 120 s or discharged.

anode and lithium iron phosphate cathode (G/LFP) show higher specific power but lower energy density than G/NMC. Cells with lithium titanium oxide (LTO) anode and NMC cathode or lithium manganese oxide (LMO) cathode have even higher power densities and lower degradation than G/LFP but lower specific energies. Finally, the supercapacitors offer the highest specific power, current rates, and cycle life, but the energy density is 32 times lower than G/NMC and six times lower than LTO/NMC.

2.1 | Hybrid Storage Systems for Electric Vessels

Even with the different ESS alternatives offered in the market, a single storage technology may not fulfil all the requirements for a specific marine application. Thus, the design of the ESS should be based on the most restrictive requirement. For example, if the HE-ESS is chosen according to the energy needed by the vessel but the maximum power is lower than the power requirements of the vessel, the capacity must be increased until the power requirements are satisfied. Similarly, an HP-ESS storage technology can be designed according to the power requirements but then specified with a higher capacity to satisfy the energy requirements. This consideration suggests that, by leveraging the strengths of two different ESS technologies, HESS can be optimised according to a selected metric (e.g., cost, volume, or weight).

The possible advantages offered by a HESS are illustrated in Figure 1 on a plane reporting the power and energy requirements.

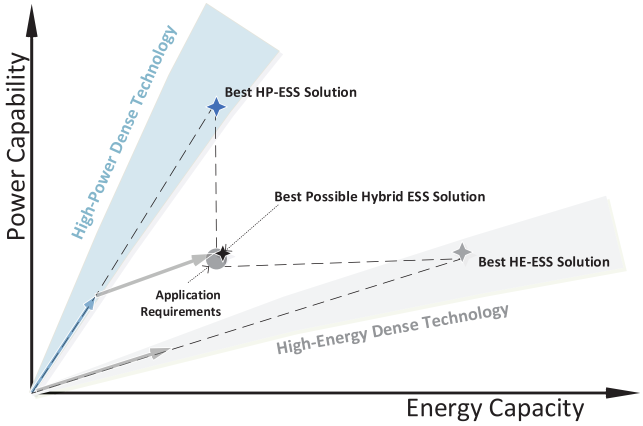

FIGURE 1 | Illustrative example of possible sizing advantages of HESS against HE-ESS and HP-ESS for specific power and energy requirements.

Two storage technologies are considered, each with very different characteristics in terms of power and energy density. It can be reasonably be assumed that the power and energy capabilities change linearly with the size of the storage system. This implies that each of the storage components will have associated capabilities lying on a line indicated in the figure as a dashed line whose slope is highlighted visually by an arrow. Assuming a required combination of power and energy capabilities indicated by the grey dot, this combination does not match either of the two storage technologies. The storage with the least power density will have to be sized based on the power requirements, resulting in an oversizing of the storage capacity (grey star in the figure). By contrast, the high-power storage component will have to be sized according to the energy capacity requirements, resulting in an oversizing of the power capability (blue star in the figure). The sizing requirements are clearly shown in the figure. A combined system can offer performance with an intermediate slope, depending on the grade of hybridization (i.e., the relative share between the two types of storage technologies). This is shown in the figure, combining the arrows and reaching a point that fulfils both the energy and the power requirements with a hybrid storage system (black star in the figure).

2.2 | Pareto Optimality Sizing

The concept of Pareto front is widely applied in multi-objective optimization and is especially valuable to restrict the domain of all possible configurations (configuration space) to the set of the configurations that present a form of optimality. In the context of this paper, it is assumed that the configuration space is represented by a large discrete set of combinations of storage capacities for the HE-ESS (E_{HE}) and HP-ESS (E_{HP}) at the beginning of life (BOL). It is also assumed that the cost function can be expressed as a monotonically increasing function of these storage capacities. This is clearly true when expressing the cost to be optimized as a function of volume, cost or weight since these quantities increase for a larger storage capacity installed. A performance index, PIx_{HESS}, could be expressed as a linear function of E_{HE} and E_{HP}, as:

$$PIx_{HESS} = \varepsilon_{xHE} \cdot E_{HE} + \varepsilon_{xHP} \cdot E_{HP} \tag{1}$$

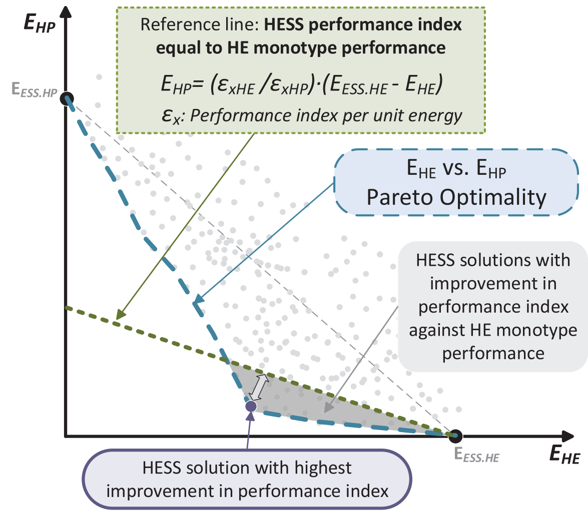

FIGURE 2 | Example of graphical detection of HESS solutions with potential improvement in a considered performance index and illustration of HESS energy pareto optimality sizing.

where ε_{xHE} and ε_{xHP} are the reference values of performance index PIx per unit energy for HE-ESS and HP-ESS reference technologies and PIx_{HESS} is the performance index evaluated for the HESS solution with installed capacities E_{HE} and E_{HP}. For example, the HESS capital cost, HESS volume and HESS weight can be estimated by replacing ε_{xHE} and ε_{xHP} by the cost per unit energy, the inverse of volumetric energy density, and inverse of gravimetric energy density, respectively, for the ESS reference technologies. Similar considerations can be extended also in the case of non-linear relations.

In this context, the concept of Pareto in the HESS-installed energy, called here the Pareto optimality sizing, can be useful to represent the set of HESS solutions with the best trade-offs between E_{HE} and E_{HP}, and therefore possible solutions with the best performance. Figure 2 shows an example of graphical detection of HESS solutions showing potential improvement in a considered performance index and an illustration of the HESS Pareto optimality sizing. The HESS solution space is defined by all the possible combinations of E_{HE} and E_{HP}, which fulfil the application requirements. This is graphically represented in Figure 2 by the grey dots together with the Pareto front as a dashed blue line. Based on the above assumptions about the cost function, any optimal configuration will lie on the Pareto front. Thus, the search for optimal configurations independent of the cost function could be restricted to the Pareto front. The point on the Pareto front corresponding to the optimal configuration will depend on the specific cost function. It should be noted that also monotype solutions are part of the Pareto front that, in the figure, correspond to the intersection of the dashed blue line with the axes.

The potential improvement of HESS solutions against monotype solutions can be estimated by finding solutions fulfilling the following criterion (assuming an improvement as a reduction in the performance index, e.g., cost, volume, or weight):

$$E_{HP} < \frac{\varepsilon_{xHE}}{\varepsilon_{xHP}} \cdot (E_{ESS.HE} - E_{HE}) \tag{2}$$

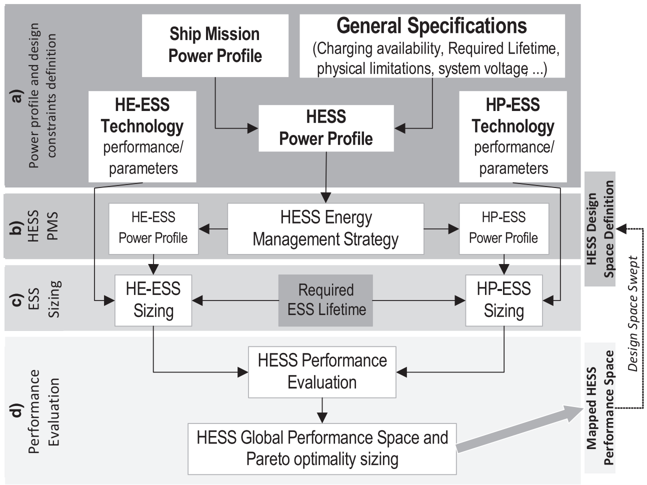

FIGURE 3 | Overview of the methodology for sizing of HESS.

This corresponds to the grey area marked in Figure 2 between the Pareto front and the green line with the assumption that the HE-ESS monotype solution offers better performance (e.g., lower cost, volume, or weight) than the HP-ESS monotype solution and that all the solutions on the green line share the same PIx_{HESS} value as the HE-ESS monotype solution. Indeed, the proposed methodology suggests restricting the focus to solutions between the Pareto front and the green line, then all the solutions/points on the right of the green line can be disregarded as they have worse performance than the best monotype solution. The optimal configuration corresponds to the points on the Pareto front with a tangent parallel to the green line. It should also be noted that if the Pareto front lies above the green line, a monotype solution should be preferred to a HESS.

3 | Methodology for the Optimal Design of HESS

The HESS under analysis is constituted by an HP-ESS and a HE-ESS, each one connected to a DC power distribution by means of a dedicated DC/DC converter. For this reason, complete control of the power flow of the two devices is allowed. As discussed in Section 2, the methodology proposed in this paper has the objective of mapping the HESS design space to the HESS performance space and obtain Pareto optimality between required installed energy for HE-ESS and HP-ESS.

The design process can be split in four main sequential steps illustrated in Figure 3 and shortly described in the following:

A. Power profile and design constraints definition: Starting from the ship mission profile and the general specifications (e.g., expected lifetime, charging availability, etc.), the HESS power profile is obtained.
B. HESS energy management strategy: The rules of the HESS energy management strategy to split the HESS power profile between the HE and HP ESSs are defined.
C. ESS sizing: The energy capacity to be installed for the HE-ESS and HP-ESS is determined considering degradation, allowed depth of discharge, and minimum lifetime.
D. HESS performance evaluation: For each sizing solution defined in step C, the performance of the HESS in terms of total installed capacity, cost, and physical size (volume and/or weight) is evaluated.

The design space domain is swept by modifying the EMS rules and testing different alternatives of HE-ESS and HP-ESS to fulfil the same HESS power profile. Consequently, steps B, C and D are repeated until the HESS global performance space is mapped. If the capacity of either the HE-ESS or HP-ESS is zero, then a single ESS is sufficient to fulfil the vessel's mission, and a HESS is not needed.

The ship mission profile can be composed of several power profiles representing different operating scenarios of the vessel, and therefore, multiple HESS power profiles need to be considered. In that case, the design space domain could be expanded as it is possible to find an optimal EMS rule for each HESS power profile and use them for the defined operating modes/scenarios of the vessel. Also, the ESS sizing should consider the associated degradation for the expected usage of each HESS power profile as well as the maximum/strongest power and energy requirements along the different HESS power profiles. These considerations are also discussed in the next subsections.

3.1 | Energy Management Strategy

As previously discussed, an energy management strategy for splitting the power between the HE and the HP ESSs must be defined. This represents a degree of freedom and should reflect a design objective. Neglecting the power converter losses, the HESS power, $P_{HESS}(t)$, can be expressed as:

$$P_{HESS}\ (t) = P_{HE}\ \ (t) + P_{HP}\ (t) \tag{3}$$

where $P_{HE}(t)$ and $P_{HP}(t)$ indicate the power allocated to the HE and HP ESSs respectively. This paper assumes a power allocation based on a saturated first-order low-pass filter. The output of the low-pass filter containing the base load is assigned to the HE-ESS while the remaining power is assigned to the HP-ESS. The discharge power is assumed as positive, thus the upper and lower filter saturation values correspond to the maximum discharge and charge power for the HE-ESS respectively. An advantage of this solution is that it can be easily implemented in a real EMS. The EMS implementation is shown in Figure 4. It should be noted that the output of the saturated low-pass filter (P_{SLPF}) is processed by a charging strategy block accounting for the necessity/opportunity to recharge the ESSs depending on the operating condition. Different *charging strategies* would lead to different ESS sizing as discussed in the following.

The low-pass filter implementation require defining three parameters: the low-pass filter cut-off frequency (ω_0), the maximum discharge power of HE-ESS ($P_{HE.DCHmx}$) and the maximum charge power of HE-ESS ($P_{HE.CHmx}$). However, only two of these parameters (ω_0 and $P_{HE.DCHmx}$) have been considered as free design parameters to guarantee the energy balance of the resulting power profiles. The parameter $P_{HE.CHmx}$ has been set as the maximum charge power required to recover the discharged energy per cycle within the available charging time of the power

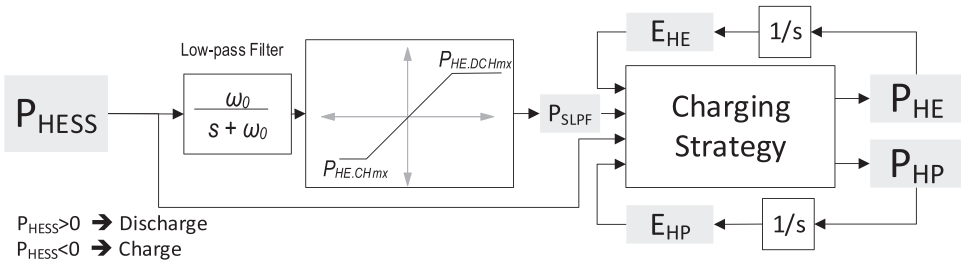

FIGURE 4 | Energy management strategy based on low pass filtering for zero-emission vessels.

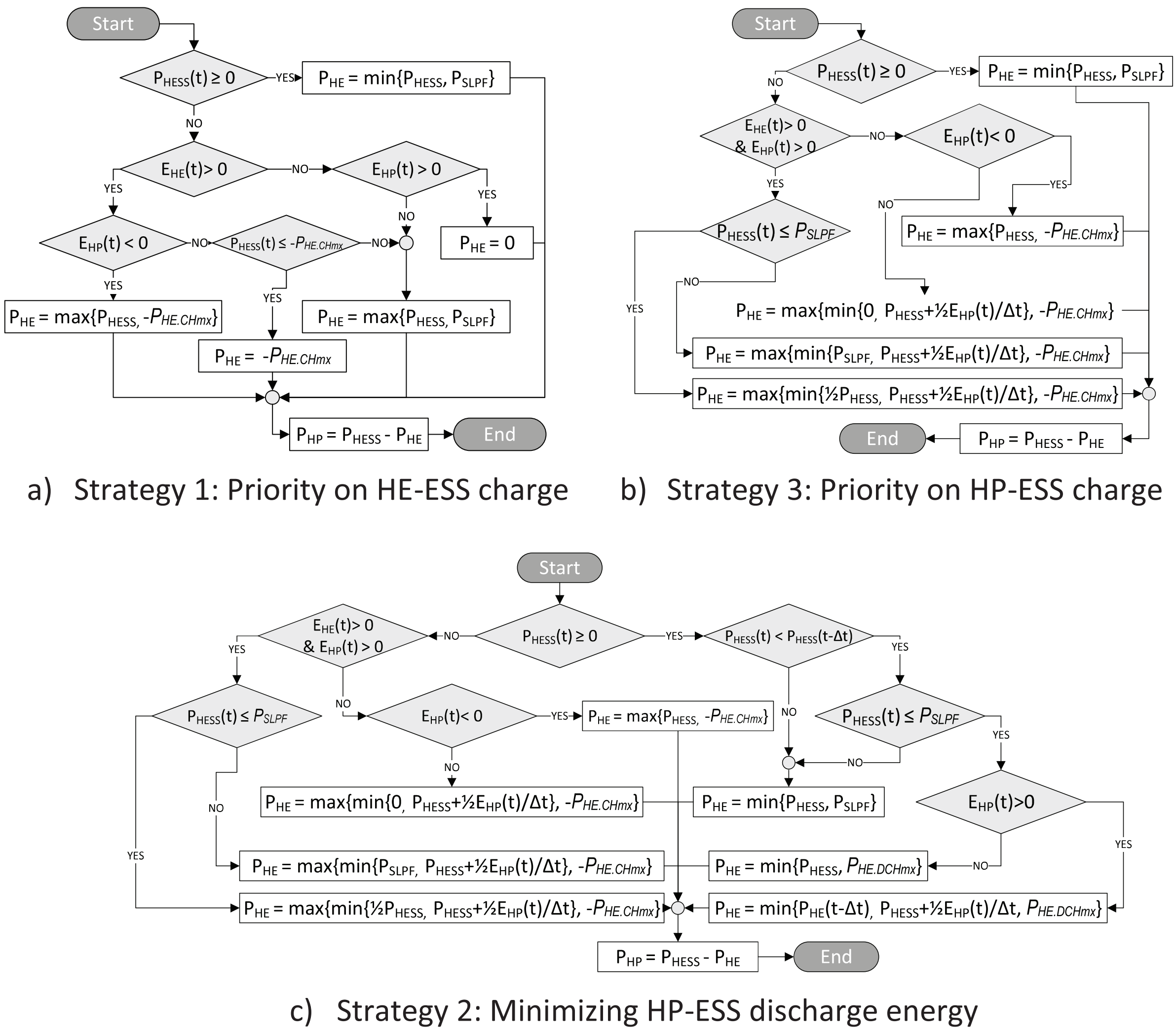

FIGURE 5 | Flowchart for the three charging strategy alternatives for the charging strategy block in the EMS (Figure 4).

profile, so e.g., if a power profile is composed of two main cycles with discharged energies per cycle of 100 and 150 kWh, and the available charging times after each discharge are 15 min and 20 min, respectively, then the required charge power by the profile is 450 kW (max{100 kWh/0.25 h, 150 kWh/0.33 h}).

3.1.1 | Charging Strategies

Three possible charging strategies are considered, and their flowcharts are shown in Figure 5. They are detailed in the following, and their effect is illustrated in Figure 6.

1. Priority on HE-ESS charge: The flowchart for this charging strategy is shown in Figure 5a. This charging strategy prioritizes the charging of the HE-ESS over the HP-ESS, while avoiding power exchange between the HP-ESS and the HE-ESS. Thus, the sign of the HP and HE ESSs powers is always consistent with the sign of the required power profile. When the HESS is discharging, the power reference for the HE-ESS follows the minimum of the output of the filter and the required power $P_{HESS}(t)$. When the HESS is charging,

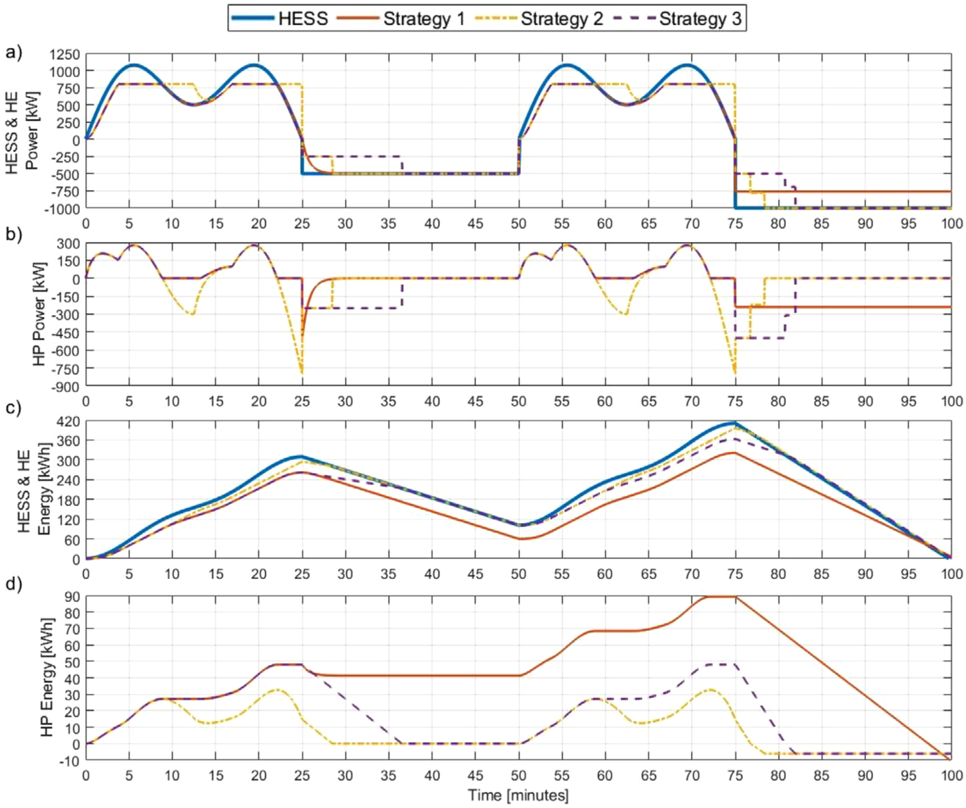

FIGURE 6 | Comparison of HESS energy management strategies (Strategy 1: Priority on HE-ESS charge; Strategy 2: Minimizing HP-ESS discharge energy; Strategy 3: Priority on HP-ESS charge). (a) HESS power and HE-ESS power; (b) HP-ESS power; (c) discharge energy for the HESS and HE-ESS; and (d) discharge energy for the HP-ESS.

the HE-ESS is charged at maximum possible power (i.e., the lowest of the available charging power and the output of the filter) until it is fully charged; then, the HP-ESS is charged at maximum available power.

2. Minimizing HP-ESS discharge energy: The flowchart for this charging strategy is shown in Figure 5c.This strategy prioritizes recovering the energy to HP-ESS right after a discharge pulse is delivered, using the HE-ESS to recharge HP-ESS when the HESS is discharging. Thus, the strategy allows the power flow from the HE-ESS to HP-ESS, but not the flow in the opposite direction. When the HESS is discharging, if the HESS required power is higher than or equal to the output of the low-pass filter, then the HE-ESS follows the output of the low pass filter, and the HP-ESS also discharges providing the remaining power; however, when the HESS required power becomes lower than the delivered power by HE-ESS ($P_{HESS}(t) < P_{HE}(t - \Delta t)$), the HE-ESS keeps delivering the same power, recharging the HP-ESS, until it is fully charged. This may result in higher average power per cycle for the HE-ESS but reduces the required energy per discharge cycle for the HP-ESS. On the other hand, when the HESS is charging, the HE-ESS follows the output of the low-pass filter but constrained to ensure that at least half of the available charging power goes to charge HP-ESS until it is fully charged.
3. Priority on HP-ESS charge: The flowchart for this charging strategy is shown in Figure 5b. This charging strategy prioritizes having the HP-ESS charged over the HE-ESS during the HESS charging phase, while avoiding power exchange between HP-ESS and HE-ESS during the HESS discharge phase. As with strategy 1, the sign of the HP and HE ESSs' powers are always consistent with the sign of the required power profile. When the HESS is discharging, this strategy follows the same principle as in discharging strategy 1. When the HESS is charging, this strategy follows the same charging rule as in charging strategy 2, prioritizing the HP-ESS charging while also charging the HE-ESS.

In the example reported in Figure 6, both power cycles present the same HESS discharge power profile, with a peak discharge power of 1075 kW. The charging power profiles are constant, but at values of 500 and 1000 kW. A saturated low-pass filter with a cut-out frequency of 3.33 mHz and a maximum discharge power of 800 kW is considered for the three charging strategies. The required usable energy for the HESS profile is 417 kWh, as shown in Figure 6c. It should also be noted that the discharge energy increases when ESS is discharged and decreases when the ESS is charged. Thus, it is possible to estimate a required usable energy (E_{req}) associated with a power profile ($P_{ESS}(t)$) by the difference between maximum and minimum discharged energy as:

$$E_{req} = \max\left(\int_0^{T_{FO}} P_{ESS}(t) \cdot dt\right) - \min\left(\int_0^{T_{FO}} P_{ESS}(t) \cdot dt\right) \quad (4)$$

where T_{FO} is the fundamental operating period of the power profile.

TABLE 2 | Summary of ESS basic requirements for the illustrative example in Figure 6.

	Requirement	Charging strategy 1	Charging strategy 2	Charging strategy 3
HE-ESS	Usable energy [kWh]	321	396	367
	RMS discharge power [kW]	663	732	663
	RMS charge power [kW]	638	757	701
	Max. charging power [kW]	760	1000	1000
HP-ESS	Usable energy [kWh]	100	39	50
	RMS discharge power [kW]	182	186	182
	RMS charge power [kW]	176	311	351
	Max. charging power [kW]	500	800	500

It can be observed from the example illustrated in Figure 6 that the selection of a given charging strategy will lead to different power and usable energy requirements for the HE-ESS and the HP-ESS, which are summarized in Table 2. It can be noted that, while using the same low-pass filter parameters, strategy 1 reduces energy and power requirements for the HE-ESS, compared to strategies 2 and 3; however, more usable energy is required for the HP-ESS with strategy 1. On the other hand, strategy 2 results in the lowest usable energy required for HP-ESS but also in strongest power and energy requirements for HE-ESS, compared to strategies 1 and 3. The different ESS requirements, together with the considered ESS technology performance, will result in different requirements for the energy capacity to be installed, as discussed in the next sub-section.

3.2 | ESS Sizing Criteria

The size of the storage elements (HE-ESS and HP-ESS) should be defined to fulfil the mission profile during the entire lifetime of the vessel. Since the ESS will lose capacity due to degradation, it should be ensured that enough ESS capacity remains during operation at end of the design life (E_{EDL}). After the EMS rule is defined, the sizing criteria presented in this section should be applied to both the HE-ESS and HP-ESS subsystems, with their associated power profiles derived from the power split procedure. The proposed ESS sizing algorithm estimates the minimum capacity to be installed, considering the following criteria:

3.2.1 | Required Usable Energy and State-Of-Charge Range

The minimum required usable energy (E_{MRU}) is equal to the maximum required usable energy from all required ESS power time series composing the mission profile, so if the mission profile is composed of N_{ts} power time series:

$$E_{MRU} = \max\left(E_{req1}, E_{req2}, \dots, E_{reqi}, \dots, E_{reqN_{ts}}\right) \tag{5}$$

where E_{reqi} is the required usable energy associated with the *i-th* ESS power time series, which can be estimated using Equation (4). Then, the ESS is sized to charge and discharge E_{MRU} at the end of design life (EDL) and while maintaining the state of charge (SoC) within the defined minimum (SOC_{mn}) and maximum (SOC_{mx}) set design limits (e.g., between 10% and 90%):

$$E_{EDL} \geq \frac{E_{MRU}}{SOC_{mx} - SOC_{mn}} \tag{6}$$

3.2.2 | Required Power Versus ESS Power Capability Degradation

Each ESS is sized considering the maximum charge and discharge rates allowed by its technology, while ensuring a charging/discharging power at least as large as the required maximum continuous (P_{MCC}/P_{MCD}) and peak (P_{MPC}/P_{MPD}) powers from all required ESS power time series composing the mission profile at the EDL. By assuming that the ESS is built by connecting n_s reference modules in series to achieve the required voltage and n_p parallel-connected strings to achieve the required capacity (Ah_{ESS}), the first-order resistive circuit model for the reference ESS module, including the ESS open circuit voltage (OCV), an internal ohmic resistance (R_0), and a RC parallel network (R_1 and C_1), can be used to approximate the correlation between ESS current (I_{ESS}) and ESS power (P_{ESS}), as follows:

$$P_{ESS} = I_{ESS} \cdot n_s \cdot \left(OCV - R_0 \cdot \frac{I_{ESS}}{n_p} - V_c\right) \tag{7}$$

$$R_1 C_1 \cdot \frac{dV_c}{dt} = R_1 \cdot \left(\frac{I_{ESS}}{n_p}\right) - V_c \tag{8}$$

where R_0 and R_1 depend on SOC, temperature, and current direction (charge or discharge), while OCV and C_1 vary with SOC. Rearranging Equation (7) to express it in terms of the nominal capacity of reference module at BOL (Ah_{REF}), the current rate ($C_{rate} = I_{ESS} / Ah_{ESS}$), the nominal energy of reference module at BOL (E_{REF}) and ESS nominal energy at BOL ($E_{BOL} \cong n_s \cdot n_p \cdot E_{REF}$):

$$\frac{P_{ESS}}{E_{BOL}} = C_{rate} \cdot \left(\frac{OCV}{V_{REF}} - \frac{R_0 \cdot Ah_{REF}^2 \cdot C_{rate}}{E_{REF}} - \frac{V_c}{V_{REF}}\right) \tag{9}$$

where V_{REF} is an average voltage obtained from the relation between nominal energy and capacity of the reference module ($E_{REF} = V_{REF} \cdot Ah_{REF}$), with the Ah_{REF} and E_{REF} values normally reported in the module datasheet.

For the estimation of the maximum continuous powers, Equation (8) can be simplified by considering state-steady response in the RC network ($V_c \approx R_1 \cdot I_{ESS}/n_p$). Then, accounting for the required maximum charging/discharging powers and the worst-case operating conditions, the following conditions should be satisfied:

$$E_{BOL} \geq \frac{P_{MCC}}{C_{rate,MCC} \cdot \left(k_{\Delta V} + k_{\Delta R} \cdot (R_{0c.MAX} + R_{1c.MAX}) \cdot C_{rate,MCC}\right)} \quad (10)$$

$$E_{BOL} \geq \frac{P_{MCD}}{C_{rate,MCD} \cdot \left(k_{\Delta V} - k_{\Delta R} \cdot (R_{0d.MAX} + R_{1d.MAX}) \cdot C_{rate,MCD}\right)} \quad (11)$$

$$k_{\Delta R} = \frac{k_{R.EOL} \cdot Ah_{REF}^2}{E_{REF}} \quad (12)$$

$$k_{\Delta V} = \frac{OCV\,(SOC_{mn})}{V_{REF}} \quad (13)$$

where $C_{rate,MCC}$, $C_{rate,MCD}$ are the maximum continuous charge and discharge rates for the reference module, respectively, $OCV(SOC_{mn})$ is the OCV estimated at SOC_{mn}, $R_{0c/d.MAX}$; $R_{1c/d.MAX}$ are the maximum expected values during charge/discharge for the resistances R_0 and R_1, respectively (typically estimated at the lowest expected module temperature and SOC_{mn}), and $k_{R.EOL}$ is the expected maximum increment of ESR at the end of life (EOL) (typically $k_{R.EOL} = 2$).

On the other hand, for the estimation of maximum peak powers, the worst-case scenario is that C_1 is charged at maximum opposite polarity of the OCV right before peak power is delivered. This happens when P_{MPC} should be delivered right after a discharge cycle at P_{MCD}, and when P_{MPD} is required during the timeframe when P_{MCD} is delivered. Then, from Equation (9), the following conditions should be also satisfied:

$$E_{BOL} \geq \frac{P_{MPC}}{C_{rate,MPC} \cdot \left(k_{\Delta V} + k_{\Delta R} \cdot \left(R_{0c.MAX} \cdot C_{rate,MPC} - R_{1c.MAX} \cdot C_{rate,MCD}\right)\right)} \quad (14)$$

$$E_{BOL} \geq \frac{P_{MCD}}{C_{rate,MPD} \cdot \left(k_{\Delta V} - k_{\Delta R} \cdot \left(R_{0d.MAX} \cdot C_{rate,MPD} + R_{1d.MAX} \cdot C_{rate,MCD}\right)\right)} \quad (15)$$

where $C_{rate,MPC}$, $C_{rate,MPD}$ are the maximum peak charge and discharge rates for the reference module, respectively, and all other parameters as previously described.

3.2.3 | Remaining Capacity Versus Capacity Degradation

The ESS capacity at BOL should be sized to ensure that after degradation, the total capacity loss at EDL ($Q_{lossEDL}$) does not reduce the ESS remaining capacity to a value lower than the energy required for the mission power profile:

$$E_{EDL} = E_{BOL} - Q_{lossEDL} \geq \frac{E_{MRU}}{SOC_{mx} - SOC_{mn}} \quad (16)$$

where $Q_{lossEDL}$ depends on calendar aging as well as on the ESS cycling use (defined mainly by depth of discharge, charge/discharge current rates and temperature), and it is estimated following the methodology described in Subsection 3.3.

3.2.4 | ESS End of Life Versus Required Design Life

The aging process in electrochemical energy storage devices (like Li-ion batteries and supercapacitors) is reflected mainly in capacity loss and the increment of internal resistance. While the methodology considers the effects of the increment in internal resistance on power capability degradation through the parameter $k_{R.EOL}$, the capacity loss has been considered the main EOL criterion in this work. Thus, the EOL criterion (k_{EOL}) for the ESS has been related to the ESS capacity fade [19]:

$$k_{EOL} = \frac{Q_{lossEOL}}{E_{BOL}} \cdot 100\% \quad (17)$$

where $Q_{lossEOL}$ is the total capacity loss at EOL. Normally, k_{EOL} values between 20% and 30% are considered for electrochemical energy storage devices, and here $k_{EOL} = 20\%$ is assumed.

Then, ESS should be sized to allow the energy cycling prescribed by the power profile without causing the ESS to reach its EOL before EDL:

$$\frac{Q_{lossEDL}}{E_{BOL}} \cdot 100\% \leq k_{EOL} \quad (18)$$

Each of the previously mentioned criteria gives a minimum required capacity to be installed, so this implies that E_{BOL} is given by the maximum of all calculated energy capacities.

3.3 | ESS Degradation Model

As the EOL criteria have been linked to the capacity fade, then the considered degradation model only considers the effects on capacity fade given by calendar aging and cycling degradation. While it assumes that the maximum capacity loss will be reached before the maximum allowed increment in internal resistance, the overall increment in ESR is considered to fulfil power requirements at EDL, as previously described in the second sizing criterion. Also, it is assumed that superposition applies, such that the incremental effect of each cycle in the overall degradation can be added, and such that incremental calendar capacity loss can be added to the capacity loss due to the cycles.

Based on the previous assumptions, the total capacity loss at EDL is estimated by:

$$Q_{lossEDL} = Q_{cal} + Q_{cycle} \quad (19)$$

where Q_{cal} is the total calendar degradation and Q_{cycle} is the total cycling degradation at the EDL, expressed in J. The calendar degradation can be estimated by:

$$\frac{Q_{cal}}{E_{BOL}} = \frac{\Delta Q_{cal}}{100} \cdot T_{EDL} \quad (20)$$

where ΔQ_{cal} is the capacity loss per year due to calendar aging (in percent of initial capacity), and T_{EDL} is the design lifetime in years.

On the other hand, the capacity loss associated with cycling degradation is estimated following the methodology described in

[19]:

$$Q_{cycle} = \sum_{i=1}^{N_{ts}} \left(N_{FOP(i)} \cdot T_{EDL} \cdot \sum_{k=1}^{N_{cycle(i)}} \Delta Q_{cyc}(i,k) \right) \quad (21)$$

where ESS has been cycled $N_{cycle(i)}$ times at different conditions associated with the *i-th* ESS power time series composing the ship mission profile, which repeats $N_{FOP(i)}$ times per year. The cycle life model based on fatigue theory reported in [26], in combination with the multi-factor cycle life prediction methodology reported in [24], has been used for the estimation of the fractional cycling degradation per cycle (ΔQ_{cyc}), expressed in J. The main assumptions used are that the impact of main operational factors on ESS cycle life is approximated to be independent of each-other, as well as that the cycling degradation is uniformly distributed along the lifetime, it follows that:

$$\Delta Q_{cyc} = \frac{Q_{cyc.ref}}{N_{CL.ref}} \cdot \left(\frac{DoD}{DoD_{ref}}\right)^{\beta} \cdot \left(\frac{I_C}{I_{C.ref}}\right)^{\alpha_C} \cdot \left(\frac{I_D}{I_{D.ref}}\right)^{\alpha_D} \cdot e^{\gamma \cdot \left(\frac{1}{T_{c.ref}} - \frac{1}{T_c}\right)} \quad (22)$$

where DoD is the depth of discharge, T_c is the average temperature, I_C and I_D are the charging and discharging current rates, respectively, β, α_C, α_D, and γ are the ESS-technology-dependent degradation stress factor fitting parameters for DoD, I_C, I_D and T_c, respectively, and $N_{CL.ref}$ and $Q_{cyc.ref}$ are the number of cycles and the associated cycling degradation (expressed in J) under reference conditions for the specific energy storage technology.

The estimated degradation stress factor parameters for each technology reported in Section 4 have been calculated using different data sources and they can be considered as representative parameters for each technology when neglecting other factors that may affect the cell degradation performance beyond the anode/cathode chemistry, as for example the shape (cylindrical, pouch, or prismatic), the cell size, the internal number of layers, and so on. Cycling performance data reported in [29–31] have been considered to estimate all stress factor parameters for LTO/NMC technology, while for LTO/LMO technology, data reported in [32] have been used. For LFP technology, cycling performance data reported in [33, 34] have been considered, while for NMC-E and NMC-P technologies, the data reported in [25, 34–37] have been considered. In the case of supercapacitors, their degradation is mainly determined by the amount of time they are kept at a given voltage and temperature [38], so degradation performance data reported in [38, 39] along with methodology reported in [40], have been considered to estimate the supercapacitor degradation stress factor parameters.

For a given power profile, the rain flow algorithm [26] has been used to estimate the equivalent energy cycles and the associated DoDs and C-rates, however the average ESS temperature cannot be determined directly. The ESS temperature performance depends on multiple factors, like the ESS cooling system and module thermal performance. A simplified approach is considered here. First, the average ESS temperature is proportional to the ESS losses. Then, by neglecting variations in the internal resistance during the cycle, the ESS temperature rise against a constant heatsink temperature ($T_{HS.REF}$) is proportional to the square of the current rates ratio. Considering the average ESS temperature per cycle (T_C) as the average temperature during charge and discharge, it is then approximated by:

$$T_C = T_{HS.REF} + (T_{C.REF} - T_{HS.REF}) \cdot \left[\frac{P_D}{P_D + P_C} \cdot \left(\frac{I_C}{I_{C.Tref}}\right)^2 + \frac{P_C}{P_D + P_C} \cdot \left(\frac{I_D}{I_{D.Tref}}\right)^2 \right] \quad (23)$$

where P_C and P_D are the equivalent/average cycle charging and discharging power, respectively.

4 | Numerical Example for An Electric Harbour Tug

4.1 | Mission Profile and General Specifications

Tugboats are relevant candidates for adopting HESS since their mission profiles are characterized by low operational hours and low utilization of the total power installed [41]. An electric tugboat with a propulsion output of 3236 kW [42] is considered in this section to illustrate the proposed HESS sizing methodology.

Figure 7 shows the standard mission profile for the tugboat, which follows the main operating data model reported in [42, 1], as well as a similar aggregated power profile as reported in [41]. The mission profile exhibits three main operation modes: transit, working, and charging. Transit mode is when the tugboat is leaving or returning from the work-point. Working mode occurs during the pulling of large ships in harbour. Charging mode refers to the tugboat being connected to the charging station at harbour. A constant charging rate of 1 MW is considered for simplicity. Figure 7a shows the power time series per trip associated with the standard tugboat mission composed of around 40 min of transit, 20 min of working, and 30 min needed to charge. Figure 7b shows the aggregated power demand associated with the discharge power in Figure 7a. The tugboat demands less than 20% of nominal power more than 70% of the time per mission [41]. Table 3 summarizes the main ESS requirements and common design constants for the considered numerical example. A total of 1680 mission/trips per year (280 operating days with 6 standard missions/trips per day) is considered, which is quite in line with the average of the typical yearly operating time (2520 h) reported in [41, 43].

4.2 | Reference ESS Performance Parameters and Monotype Solutions

The feasibility of adopting an HESS topology for this application depends on the performance comparison to a reference ESS solution based on a single ESS technology (an ESS monotype solution). To establish the best reference ESS monotype solution, the ESS technologies commonly used in marine applications have been considered. Table 4 summarizes the main ESS technology parameters needed for the ESS sizing methodology, taking as reference the ESS technologies presented in Table 1 and complementary ESS performance data reported from the literature [44, 45]. The ESS reference performance parameters related to volume and weight consider extra components (like BMS, cooling

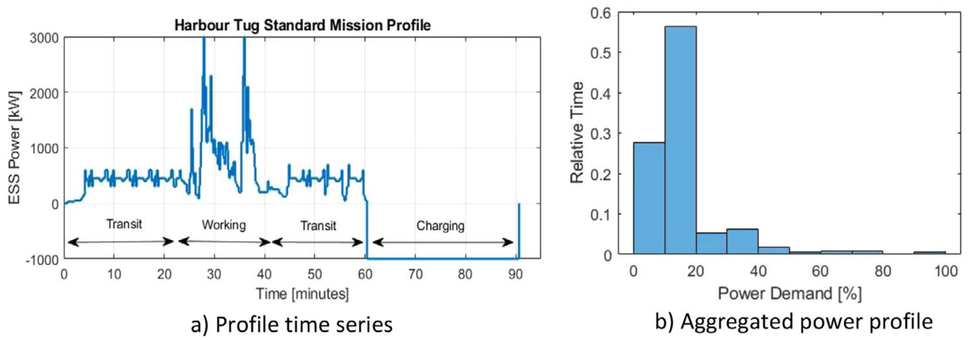

FIGURE 7 | Electric harbour tug: standard mission profile. Nominal propulsion power 3,236 kW.

TABLE 3 | ESS general specifications.

Harbour tug mission requirements			
Minimum usable energy [kWh]	500	Typical yearly operating time [41, 43] [h]	1000–4000
Max. RMS charge power (120 s) [kW]	1000	Assumed mission/trips per year	1680
Max. RMS discharge power (120 s) [kW]	1800	Assumed operating time for this profile [h]	2520
Max. RMS discharge power (10 min) [kW]	1300	Peak charge power [kW]	1000
Max. RMS discharge power (1 h) [kW]	650	Peak discharge power [kW]	3000
ESS design constants			
Minimum lifetime [years]	10	Reference heatsink temperature [°C]	20
Safety margin in peak current [%]	30	Reference ESS temperature at max. C-rates [°C]	45
Safety margin in continuous current [%]	15	Capacity fade to EOL [%]	20

pipelines, the cabinet/enclosure and so on), which decrease the energy density compared to a single ESS module/cell.

The design of the capacity of HE ESS technologies is mainly dictated by the need to avoid EOL before EDL and/or according to the required C-rates, while for HP technologies the predominant criterion is to ensure enough remaining capacity at EDL. Required installed capacity for HP-ESStechnologies is lower compared to HE ESS technologies; however, they have higher cost, volume, and weight per unit energy. Figure 8 shows the monotype ESS sizing results and associated performance (cost, volume, and weight) as a function of harbour tug missions/trips per year for the considered ESS technologies. It can be noted that the monotype ESS solution based on supercapacitors requires the lowest installed capacity among the considered ESS technologies, however the ESS cost, volume, and weight associated with the required capacities for supercapacitors are the highest compared with the other technologies.

Regarding the ESS cost, the G/LFP-P technology provides the best alternative for any required number of trips per year; however, higher volume and weight are required compared with G/NMC-P solutions, which provide the solutions with the lowest volume and weight among the compared technologies. Also, G/NMC-P ESS should be sized according to the required peak C-rates; and therefore, the sizing becomes independent of harbour tug usage (number of missions per year), making this solution the best for heavy-duty profiles.

When 1680 missions/trips per year are considered. It can be noted that the cost of the G/NMC-P solution is around 28% higher than the cost of the G/LFP-P solution, but the G/NMC-P solution provides the lowest volume and weight, with a reduction of 35% in volume and 40% in weight compared to the G/LFP-P solution. Also, the estimated State Of Health (SOH) at EDL for G/NMC-P solution is 87%, so a longer lifetime can also be expected for this solution, which has been estimated to be around 15 years to reach EOL. Given that harbour tugs have strong volume and weight constraints, G/NMC-P technology seems to be the best alternative for monotype ESS solutions.

4.3 | HESS Solutions

The proposed HESS sizing methodology has been applied to find relevant HESS solutions for the electric tug profile, by combining of ESS technologies listed in Table 4 and considering the general specifications in Table 3.

Figure 9 shows the obtained HESS energy performance space for six relevant combinations of ESS technologies. For each case, the HESS performance space has been mapped by sweeping the three free EMS parameters: the low-pass filter cut-off frequency between zero and infinity, the maximum discharge power of HE-ESS between 400 kW and 3000 kW, and evaluating the three charging strategies discussed in Section 3.1. A total of

TABLE 4 | Reference ESS technology parameters.

Technology		G/NMC-E	G/LFP-E	G/LFP-P	G/NMC-P	LTO/LMO	LTO/NMC	SuperCap.
Discharge current rate [C-rate] (cont./peak)		1/2	2/3	4/6	3/5	7/13	20/36	124/380
Charge current rate [C-rate] (cont./peak)		0.5/1	1/2	4/6	3/5	7/13	20 / 36	124/380
Ref. resistance factor ($k_{\Delta R}$) [s/Ω]		3.1338	3.4595	2.7692	5.7996	6.1653	0.289	0.0362
Ref. voltage factor ($k_{\Delta V}$)		0.9403	0.969	0.969	0.9531	1	0.98	0.5507
Max. charge/discharge R_0 [mΩ]		5.6/5.6	8.8/8.8	2.56/2.56	3.7/3.7	3/2,87	12/12	8.7/8.7
Max. charge/discharge R_1 [mΩ]		2.8/5.6	4.4/4.4	1.28/1.28	1,85/1,85	1.5/1.43	6/6	4.3/4.3
System specific energy [Wh/kg]		125	73	50	76	40	24	4.5
System energy density [Wh/dm3]		115	95	65	88	45	32	3
Usable energy (SOC range) [%]		85	80	80	80	90	85	85
ESS Cost [EUR/kWh]*		400	350	550	800	1200	1500	5000
Calendar degradation [%/year]		1,00	1,11	0.95	0.91	0,80	0.80	0.71
Cycle Life*	Cycles to 80%SOH.	4000	4000	6000	10,000	25,000	60,000	1,000,000
	Reference DoD [%]	80	80	80	80	100	60	75
	Ref. Charge/discharge rates	0.3/0.3	0.2/0,2	0.8/0.8	1.2/1,2	2/2	5/5	15/15
	Ref. temperature [°C]	25	25	25	30	25	45	35
	DoD stress factor, β	1,6844	2.1327	2.1327	2.2093	2.1314	1,7113	2.8644
	Charge rate stress factor, α_C	1.6185	0.74386	0.74386	1.1162	−0.58012	−0.58012	−1
	Discharge rate stress factor, α_D	0.9180	1.3382	0.74386	0.5584	−0.58012	−0.58012	−1
	Temperature stress factor, γ [K]	3664	3684	3684	8266	4650	6495	6976

*Assumed based on similar ESS performance and literature [44, 45].

15,600 power split alternatives have been evaluated for each case reported in Figure 9. Each subplot in Figure 9 includes all the obtained discrete solutions for the HESS (plotted with circular marks), which are composed of the installed energy for HE-ESS (x-axis) and the corresponding HP-ESS (y-axis) for all the evaluated power split alternatives obtained after the ESS sizing process described in Section 3.2. Also, an area representing the possible/relevant HESS solution space is included, which is constrained on its lower borders by the obtained Pareto optimality sizing and in addition, for easy viewing purposes, its upper borders have been constrained by the square sum of normalized capacities ($(E_{HE}/E_{ESS.HE})^2 + (E_{HP}/E_{ESS.HP})^2 < 1$). Each point of the possible HESS solutions is plotted following a colour scale relative to the cost of the monotype HE-ESS solution, which is the one intercepting the x-axis. Five lines are also plotted for each case: the grey-solid line represents the minimum energy at EDL to fulfil the mission profile without going out of the maximum SOC range; the dark-grey-dashed line represents HE-HP energy combinations in proportion to the required energy of monotype HE and HP solutions; and the other three lines represent HE and HP energy combinations that produce the same cost, volume and weight than HE-ESS monotype solution, respectively. So, if there are HESS solutions below any of these lines, then these solutions bring a reduction in cost, volume or weight compared as the HE-ESS monotype solution.

The first relevant ESS combination to check follows the combination of the highest energy-dense ESS technology and the highest power capability ESS technology listed in Table 4, i.e., G/NMC-E combined with supercapacitors, which is plotted in Figure 9a. It can be noted that all HESS solutions in this case will have higher cost, volume, and weight compared with the G/NMC-E monotype solution, so combining these two ESS technologies is not convenient for the tug. This can be interpreted by the fact that G/NMC-E batteries are sized to avoid EOL before EDL, mainly driven by ESS degradation, and the reduction in HE-ESS degradation obtained by introducing HP-ESS is not significant compared to the extra energy introduced by the HP-ESS. Similar results have been observed from the combination of G/LFP-E batteries with supercapacitors, and, for combinations of G/NMC-E or G/LFP-E batteries with LTO/NMC batteries, which have not been plotted for brevity.

Figure 9b,c show the HESS energy for G/LFP-P batteries combined with supercapacitors and LTO/NMC batteries, respectively. It can be observed that, similarly to the previous case, the

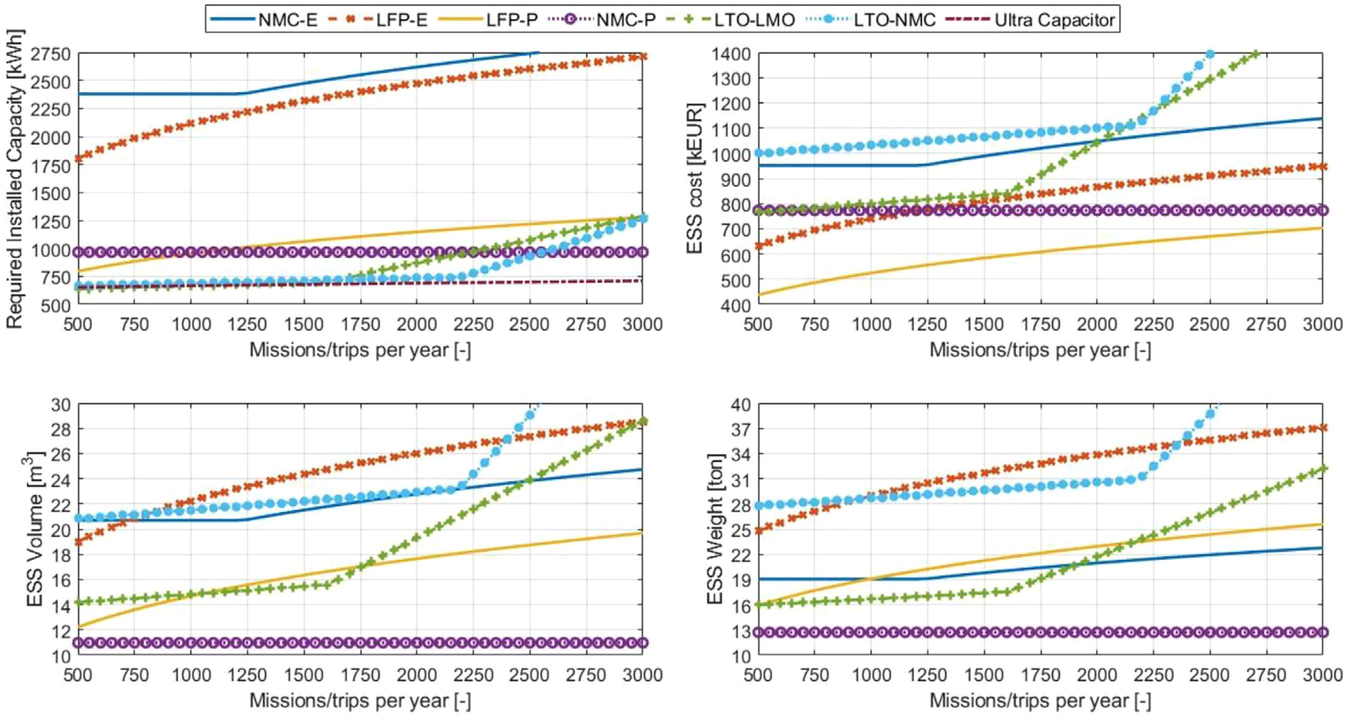

FIGURE 8 | Comparison of monotype ESS sizing results and performance against harbour tug missions/trips per year. Supercapacitors not included in the plots (ESS cost > 3260 k€, volume > 217 m^3 and weight > 145 tons).

combination with supercapacitors is not convenient for the tug. For G/LFP-P and LTO/NMC batteries, it can be noted from Figure 9 that there are HESS solutions with similar volume and weight but higher cost than the G/LFP-P monotype solution, making this combination not relevant for this application. The reason behind these results is that also G/LFP-P batteries are mainly sized to avoid EOL before EDL.

Finally, HESS results from the combination of G/NMC-P with supercapacitors, LTO/NMC and LTO/LMO, batteries are shown in Figure 9d–f, respectively. It can be noted that HESS solutions based on G/NMC-P bring improvements in cost, volume, and weight compared with the G/NMC-P monotype solution, for all three considered HP-ESS combination alternatives. Contrary to the previous cases, the G/NMC-P monotype solution is sized according to the required peak C-rate, so using the HP-ESS to reduce the required peak power for the G/NMC-P ESS also directly reduces the required energy. Given that the tug profile is characterized by short-term power peaks, the required energy of HP-ESS to supply the peak power is small, allowing HP-ESS to be used at high C-rates, taking full advantage of its high-power capability properties.

Figure 10 shows the Pareto optimality curve for the HESS solutions combining G/NMC-P with other ESS technologies with higher power capability, and the associated minimum HESS cost, volume, and weight normalized to the G/NMC-P monotype solution values. It can be noted that the Pareto optimality curve is characterized by two main slopes in all three cases. The first slope is for G/NMC-P installed energy from 966 kWh to around 720–780 kWh, and it is mainly determined by the power capability of the HP-ESS technology. For any additional HP-ESS energy, the required C-rates of G/NMC-P ESS are lower and, therefore, the reduction of the required energy of the HE ESS is larger than the additional energy of the HP ESS. For the combination with supercapacitors, a reduction in G/NMC-P required energy of 74 kWh per kWh of installed supercapacitor energy can be achieved, while for LTO/NMC and LTO/LMO this is around 7 kWh and 2.25 kWh per kWh of HP energy, respectively. The reductions in HESS cost, volume and weight follow the HE installed energy reductions in this range, and the minimum values are reached for HE installed capacities of 775 kWh, 759kWh, and 734 kWh for the combination with supercapacitors, LTO/NMC, and LTO/LMO, respectively.

Above a certain capacity of HP, the slope changes because the C-rates of G/NMC-P are sufficiently low to the point that EDL becomes the dominant sizing criterion. For the combination with supercapacitors and for HE-ESS installed capacities below 775 kWh, both systems should be sized to ensure enough capacity at EDL, and a reduction of around 1.5 kWh in G/NMC-P required installed capacity per kWh of installed supercapacitor capacity can be achieved in this range. For the combination with LTO/NMC and LTO/LMO, two sizing criteria are alternatively used to ensure enough capacity at EDL or avoid EOL before EDL, so the trends are not as straight as for supercapacitors (Figure 10). A reduction of installed capacity of around 1.26 kWh and 0.68 kWh per kWh installed HP-ESS energy can be achieved for the combination with LTO/NMC and LTO/LMO, respectively.

Table 5 summarizes the results discussed so far. The lowest HESS cost and weight are achieved with supercapacitors, with a reduction in cost and weight of about 18% and 15%, respectively, compared with the G/NMC-P monotype solution. The lowest HESS volume is achieved for the combination of

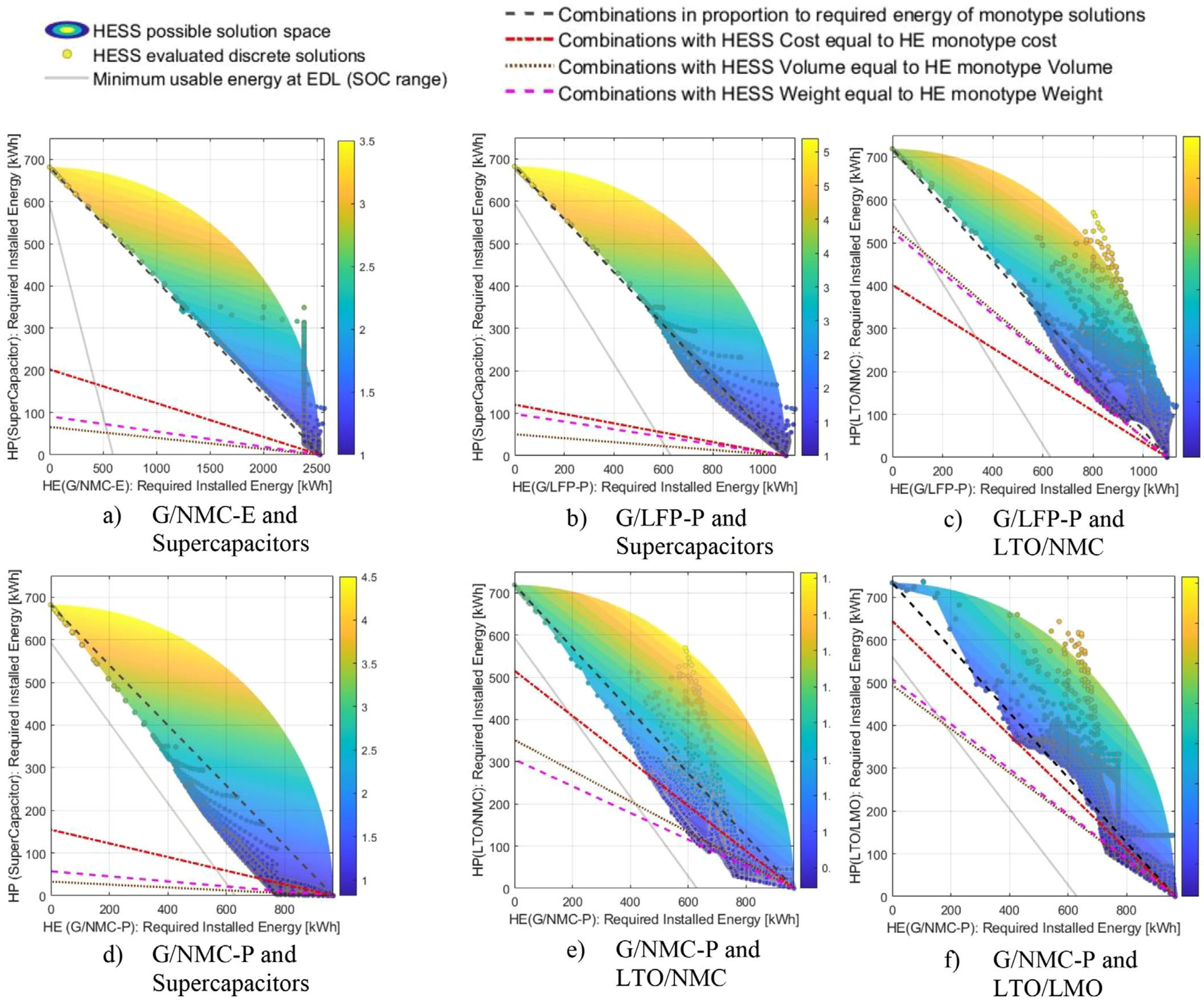

FIGURE 9 | HESS energy performance space for relevant combinations of ESS technologies. For each subfigure, the colour scale represents the relative cost of HESS solutions respect to HE-ESS monotype solution (which is the one intercepting the x-axis).

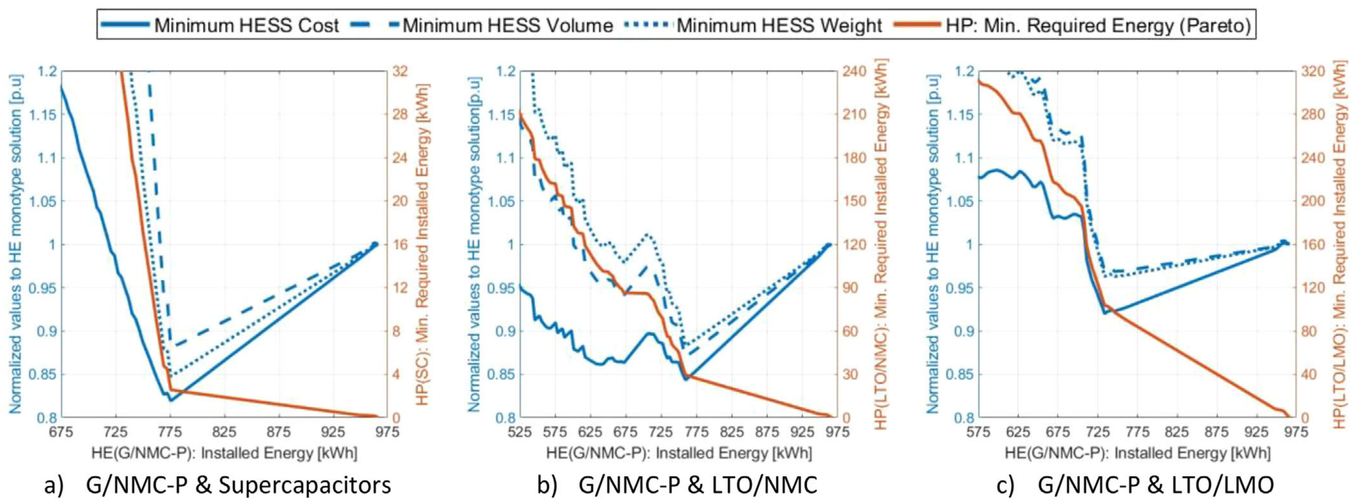

FIGURE 10 | HESS energy Pareto optimality and associated HESS cost, volume and weight for the combination of G/NMC-P LiBs and higher power capability technologies.

TABLE 5 | HESS solutions with best performance for G/NMC-P combined with HP-ESS. (values in parenthesis show reductions with respect to reference G/NMC-P monotype solution).

HP-ESS technology		Supercapacitors	LTO/NMC	LTO/LMO
Installed energy [kWh]	G/NMC-P	775.45 (−19%)	758.96 (−21%)	733.60 (−24%)
	HP-ESS	2.58	29.59	103.39
Capital Cost [k€]		633 (−18%)	651 (−16%)	711 (−8%)
Volume [m^3]		9.69 (−12%)	9.57 (−13%)	10.64 (−3%)
Weight [Tons]		11.02 (−15%)	11.47 (−12%)	12.51 (−4%)
SOH at EDL [%]	G/NMC-P	81.3	81.5	81.7
	HP-ESS	84.4	80	80
Sizing criteria	G/NMC-P	To ensure enough capacity at EDL	To ensure enough capacity at EDL	
	HP-ESS		To avoid EOL before EDL	
Low pass filter frequency [mHz]		64.12	33.60	14.98
Limit HE discharge power [kW]		2399.3	2355.0	2268.9
Charging Strategy		Minimizing HP-ESS discharge energy	Priority on HP-ESS charge	

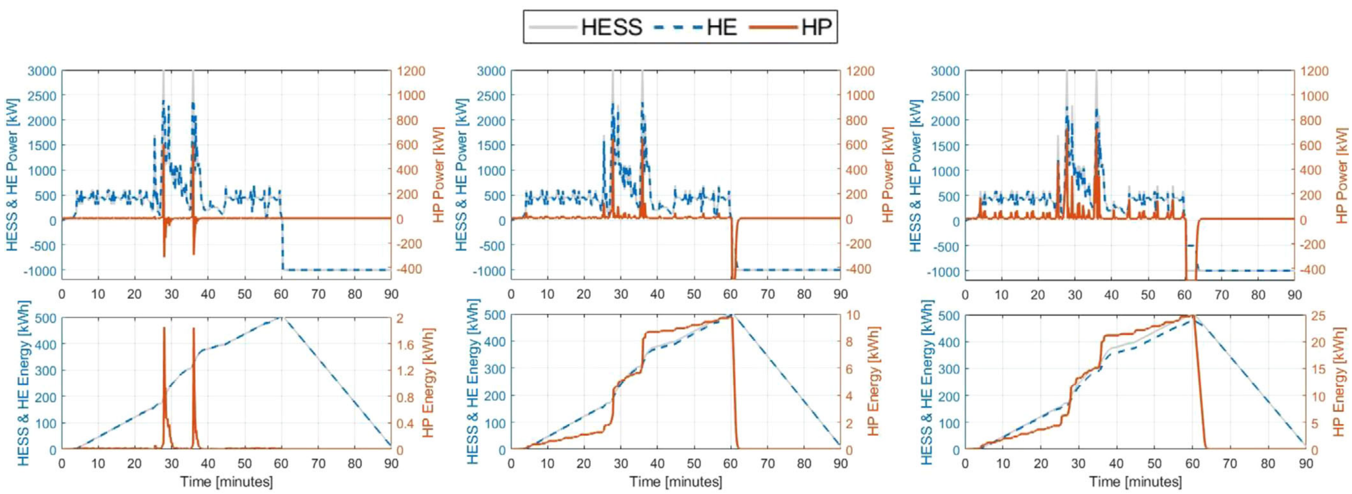

a) G/NMC-P & Supercapacitors b) G/NMC-P & LTO/NMC c) G/NMC-P & LTO/LMO

FIGURE 11 | HESS power profiles for the solutions listed in Table 5.

G/NMC-P with LTO/NMC, with a reduction in volume of about 13% respect to the G/NMC-P monotype solution, while the HESS with supercapacitors achieves a 12% reduction in volume.

Figure 11 shows the power profiles associated with the HESS solutions listed in Table 5. For supercapacitors, the energy management strategy recharges the supercapacitor itself after every intervention. This is because the maximum sizing criterion is based on ensuring that the capacity is sufficient at EDL, which means that the total energy discharged after every peak is minimised if the supercapacitor is recharged immediately after. HP LiBs are instead only charged at the end of the cycle because, in this case, the maximum sizing criterion is based on ensuring that EOL does not occur before EDL. Thus, avoiding the additional stress (and associated degradation) of charging HP-ESS with energy from HE-ESS during the main discharge phase is preferable.

Finally, Figure 12 shows the impact of the EMS charging strategy on the Energy-Pareto optimality and the minimum achieved HESS cost for G/NMC-P combined with supercapacitors, LTO/NMC, or LTO/LMO technologies. It can be noted that, depending on the G/NMC-P installed energy, a charging strategy can become more beneficial than the others. For the analysed harbour tug profile, minimizing the HP-ESS discharge energy seems to be more beneficial to install a smaller energy capacity of HP-ESS and using it with higher C-rates, especially for the supercapacitors because they need to be sized to ensure enough capacity at EDL, but HP-LiBs are mostly sized to avoid EOL before EDL or following C-rate requirements in some cases. However, when the degradation criteria become more relevant than C-rate requirements for G/NMC-P, then the extra stress associated with transfering energy from HE-ESS to HP-ESS when trying to minimize the HP-ESS discharge energy will create more degradation, and therefore a higher slope (almost of 90°) in the energy Pareto for strategy 2 can be observed in all cases.

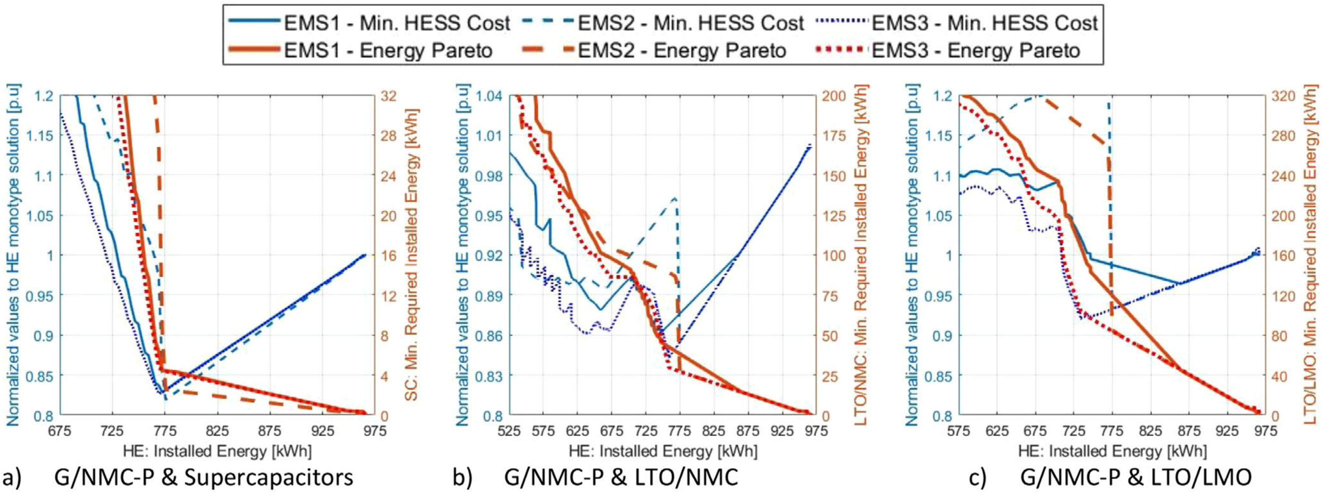

FIGURE 12 | Impact of EMS charging strategy on the Energy-Pareto optimality and minimum HESS cost for the combination of G/NMC-P and higher power capability ESS technologies.

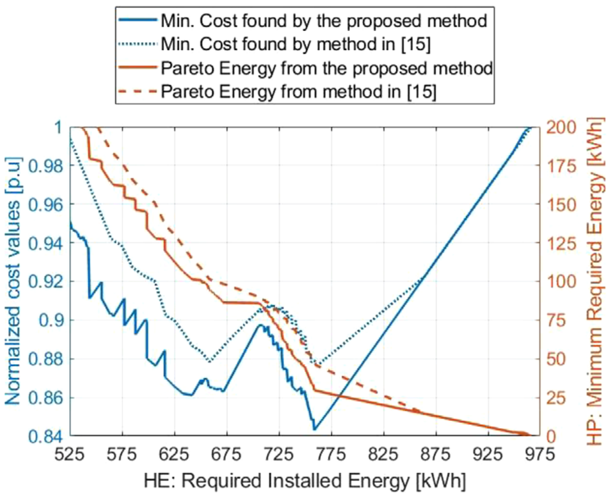

FIGURE 13 | Comparison of proposed methodology with method reported in [15]. Found Energy-Pareto optimality and minimum HESS cost for the combination of G/NMC-P and LTO/NMC.

Additionally, the method proposed in [15] has been used as a reference to compare the effectiveness of the proposed approach. The EMS used in [15] has been implemented and incorporated within the proposed HESS design framework. Figure 13 shows and compares the energy-Pareto optimality and minimum HESS cost for the combination of G/NMC-P and LTO/NMC found by the proposed methodology and the method reported in [15]. It can be noted that HESS solutions with a better trade-off can be found by the proposed EMSs compared with the one proposed in [15].

5 | Conclusions

A key challenge in design optimisation methods for fully electric vessels with multiple types of energy storage is the need to analyse a large number of cases each time the cost function used for the optimisation is modified. This paper advances the current state of the art by introducing a Pareto-based design optimisation method, applied to hybrid energy storage for zero-emission vessels. The proposed approach is more effective because it decouples the analysis of solutions that fulfil operational constraints from the optimisation process. The energy Pareto front contains all optimal configurations, independent of the cost function, allowing the search for any optimal configuration to be restricted to the Pareto front alone. This significantly reduces the computational burden, especially for evaluating again the optimal configuration when the cost function or its parameters are modified compared to conventional optimisation techniques. Moreover, the Pareto front provides a valuable graphical interpretation of the optimisation process and the robustness of the selected optimal configuration. The proposed optimisation method has been applied to an electric tugboat to demonstrate how the optimal solution with the minimum weight can be identified for a specific capacity degradation of the energy storage. This criterion is important for vessels because often batteries are designed according to this criterion and are often overdesigned to satisfy the requirements for minimum life. The example has shown that using the proposed method it is possible to obtain a design that respects the requirements and has lower volume and cost than a design solely based on batteries. The method is also applicable to other energy systems involving multiple types of energy storage, such as rail and automotive applications, where different cost functions must be tested before finalizing the design. Future research will integrate more refined models for the losses in the power converters, as they are variable with the power of the energy storage and can have different impacts on the batteries and short-term energy storage. Also, it will be explored the possibility of turning the converter off when the high-power energy storage is not in use to eliminate converter's switching losses during idling.

Author Contributions

Rene A. Barrera-Cardenas: conceptualization, data curation, formal analysis, investigation, methodology, software, visualization, writing – original draft, writing – review and editing. **Salvatore D'Arco**: conceptualization, formal analysis, funding acquisition, project administration, writing – original draft, writing – review and editing. **Luigi Piegari**: formal analysis, writing – original draft, writing – review and editing. **Pietro Tricoli**: writing – review and editing.

Acknowledgements

This paper presents results linked to research activities within Vessel Advanced Clustered and Coordinated Energy Storage Systems project (V-ACCESS) funded by Horizon Europe Program (clean and competitive solutions for all transport modes), grant agreement 101096831.

Conflicts of Interest

Two co-authors are Guest Editors of the themed issue where this paper is submitted.

Data Availability Statement

The data that support the findings of this study are available from the corresponding author upon reasonable request.

References

1. S. t. C. Hoedemaker, "Solutions for large batteries for waterborne transport, D2.1–Application Matrix," SEABAT—EU HORIZON 2020 PROGRAMME, Delft, 2021.

2. S. Nasiri, M. Parniani, and S. Peyghami, "A Multi-objective Optimal Power Management Strategy for Enhancement of Battery and Propellers Lifespan in All-Electric Ships," *Journal of Energy Storage* 65 (March 2023): 107183.

3. F. Balsamo, C. Capasso, and O. Veneri, "Performance Evaluation of an All-Electric Waterbus Supplied by Hybrid Energy Storage Systems," in *2018 International Symposium on Power Electronics*, Electrical Drives, Automation and Motion (SPEEDAM) (2018).

4. J. P. Trovão, F. Machado, and P. G. Pereirinha, "Hybrid Electric Excursion Ships Power Supply System Based on a Multiple Energy Storage System," *IET Electrical Systems in Transportation* 6, no. 3 (2016): 190–201.

5. P. G. Papageorgiou, K. O. Oureilidis, and G. C. Christoforidis, "A Systematic Review of Hybrid Superconducting Magnetic/Battery Energy Storage Systems: Applications, Control Strategies, Benefits, Limitations and Future Prospects," *Renewable and Sustainable Energy Reviews* 183 (2023): 113436.

6. A. S. Veerendra, M. R. B. Mohamed, and F. P. Garcia Márquez, "Energy Management Control Strategies for Energy Storage Systems of Hybrid Electric Vehicle: A Review," *Energy Storage* 6, no. 1 (2024): e573.

7. R. Ruchika and D. K. Jain, "A Brief Review on Hybrid Energy Storage Systems for Microgrid Application," *Przegląd Elektrotechniczny* 1, no. 4 (2023): 70–76.

8. E. Jesacher, Y. E. Bouvier, A. J. Hanschek, A. Stanojević, and P. J. Grbović, "Review on the State of the Art of Hybrid Energy Storage Systems for Electric Transportation Systems and the Applicability to Mobile Robots," in *22nd International Symposium on Power Electronics (Ee)* (2023).

9. N. G. Chatzigeorgiou, S. Theocharides, G. Makrides, and G. E. Georghiou, "A Review on Battery Energy Storage Systems: Applications, Developments, and Research Trends of Hybrid Installations in the End-User Sector," *Journal of Energy Storage* 86 (2024): 111192.

10. A. Clemente, P. Arias, L. Gevorkov, et al., "Optimizing Performance of Hybrid Electrochemical Energy Storage Systems Through Effective Control: A Comprehensive Review," *Electronics* 13, no. 7 (2024): 1258.

11. A. Rammohan and N. Kumaresan, "A Comprehensive Review on Energy Management Strategies of Hybrid Energy Storage Systems for Electric Vehicles," *Journal of the Brazilian Society of Mechanical Sciences and Engineering* 46, no. 3 (2024).

12. A. Berrada and A. Emrani, "A Comprehensive Review on Techno-Economic Assessment of Hybrid Energy Storage Systems Integrated With Renewable Energy," *Journal of Energy Storage* 84 (2024).

13. A. Nasir and A. Urooj, "Review of Hybrid Energy Storage Systems for Hybrid Electric Vehicles," *World Electric Vehicle Journal* 15, no. 8 (2024).

14. R. Ramesh and C. V. M. Gopi, "Review of Battery-Supercapacitor Hybrid Energy Storage Systems for Electric Vehicles," *Results in Engineering* 24 (2024): 103598.

15. M. Akbarzadeh, J. De Smet, and J. Stuyts, "Battery Hybrid Energy Storage Systems for Full-Electric Marine Applications," *Processes* 10, no. 11 (2022): 2418.

16. H. Rezaei, S. E. Abdollahi, S. Abdollahi, and S. Filizadeh, "Energy Managment Strategies of Battery-Ultracapacitor Hybrid Storage Systems for Electric Vehicles: Review, Challenges, and Future Trends," *Journal of Energy Storage* 53 (June 2022): 105045.

17. H. Lei, K. Li, and B. Chong, "A Review of Hybrid Energy Storage System for Heavy-Duty Electric Vehicle," *Transportation Research Procedia* 70 (2022): 234–240.

18. A. Boveri, F. Silvestro, M. Molinas, and E. Skjong, "Optimal Sizing of Energy Storage Systems for Shipboard Applications," *IEEE Transactions on Energy Conversion* 34, no. 2 (June 2019): 801–811.

19. R. Barrera-Cardenas, O. Mo, and G. Guidi, "Optimal Sizing of Battery Energy Storage Systems for Hybrid Marine Power Systems," in *2019 Electric Ship Technologies Symposium (ESTS)* (2019).

20. K. Kim, J. An, K. Park, G. Roh, and K. Chun, "Analysis of a Supercapacitor/Battery Hybrid Power System for a Bulk Carrier," *Applied Sciences* 9, no. 8 (2019): 1547.

21. F. Balsamo, C. Capasso, D. Lauria, and O. Veneri, "Optimal Design and Energy Management of Hybrid Storage Systems for Marine Propulsion Applications," *Applied Energy* 278 (2020): 115629.

22. J. N. Forestieri and M. Farasat, "Energy Flow Control and Sizing of a Hybrid Battery/Supercapacitor Storage in MVDC Shipboard Power Systems," *IET Electrical Systems in Transportation* 10, no. 3 (2020): 275–284.

23. Z. Tao, R. Barrera-Cardenas, M. Akbarzadeh, O. Mo, J. De Smet, and J. Stuyts, "Design and Evaluation Framework for Modular Hybrid Battery Energy Storage Systems in Full-Electric Marine Applications," *Batteries* 9, no. 5 (2023): 250.

24. V. Muenzel, J. de Hoog, M. Brazil, A. Vishwanath, and S. Kalyanaraman, "A Multi-Factor Battery Cycle Life Prediction Methodology for Optimal Battery Management," in *2015 ACM Sixth International Conference on Future Energy Systems* (2015): 57–66.

25. J. Nájera, J. Arribas, R. d. Castro, and C. Núñez, "Semi-Empirical Ageing Model for LFP and NMC Li-Ion Battery Chemistries," *Journal of Energy Storage* 72, no. Part A (2023): 108016.

26. S. N. Motapon, E. Lachance, L.-A. Dessaint, and K. Al-Haddad, "A Generic Cycle Life Model for Lithium-Ion Batteries Based on Fatigue Theory and Equivalent Cycle Counting," *IEEE Open Journal of the Industrial Electronics Society* 1 (2020): 207–217.

27. K. Miettinen, "*Nonlinear Multiobjective Optimization*," (Springer: New York, 1998).

28. M. U. Mutarraf, Y. Terriche, M. Nasir, K. A. K. Niazi, J. C. Vasquez, and J. M. Guerrero, "Hybrid Energy Storage Systems for Voltage Stabilization in Shipboard Microgrids," in *9th International Conference on Power and Energy Systems (ICPES)* (2019).

29. M. Soltani, S. B. Vilsen, A.-I. Stroe, V. Knap, and D.-I. Stroe, "Degradation Behaviour Analysis and End-of-Life Prediction of Lithium Titanate Oxide Batteries," *Journal of Energy Storage* 68, no. 15 (2023): 107745.

30. M. S. Hosen, T. Kalogiannis, J. Jaguemont, M. Berecibar, and J. V. Mierlo, "A Fast-Charging Study on the Lifetime of Power-Optimized Lithium Titanite Batteries by Electrochemical Impedance Spectroscopy," *ECS Meeting Abstracts* MA2020-02, no. 3 (2020): 545.

31. Toshiba Corporation, *SCIB Cell Characteristics* (Toshiba Corporation), https://www.scib.jp/en/knowledge/simulation/cell-characteristics.html. [Accessed 05 04 2024].

32. ALTAIRNANO, *24 V /70 Ah Battery Module Datasheet—Document Number: 3342112(R4)* (Altairnano: Reno, USA, 2022).

33. SAFT, *Seanergy Module Datasheet—Document Number: 35016-0617* (SAFT Specality Battery Group, Levallois-Perret, 2017).

34. S. N. Motapon, E. Lachance, L.-A. Dessaint, and K. Al-Haddad, "A Generic Cycle Life Model for Lithium-Ion Batteries Based on Fatigue Theory and Equivalent Cycle Counting," *IEEE Open Journal of the Industrial Electronics Society* 1 (2020): 207–217.

35. Freudenberg E-Power Systems /XALT Energy, *XPAND Modular Pack—XMP 123E High Energy* (Freudenberg E-Power Systems, 2024).

36. Freudenberg E-Power System /XALT Energy, *XPAND Modular Pack—XMP 96P High Power* (Freudenberg E-Power System, 2024).

37. S. F. Schuster, T. Bach, E. Fleder, et al., "Nonlinear Aging Characteristics of Lithium-Ion Cells Under Different Operational Conditions," *Journal of Energy Storage* 1 (June 2015): 44–53.

38. SKELETON Technologies, *SkelCap User Manual* (SKELETON Technologies, Estonia, 2017).

39. S. Vlasta, S. Josef, M. Jiri, et al., "Supercapacitor Degradation Assesment by Power Cycling and Calendar Life Tests," *Metrology and Measurement Systems* 23, no. 3 (2016): 345–358.

40. P. Kreczanik, P. Venet, A. Hijazi, and G. Clerc, "Study of Supercapacitor Ageing and Lifetime Estimation According to Voltage, Temperature and RMS Current," *IEEE Transactions on Industrial Electronics* 61, no. 9 (2014): 4895–4902.

41. ABB, *The ABB ElectricTug: Electric and Hybrid Tug—Analysis* (ABB Inc., Houston, 2022).

42. S. Koichi, M. Syunichi, and K. Masanori, "Development of the Hybrid Tugboat System," *IHI Engineering Review* 48, no. 1 (2015): 23–28.

43. Caterpillar Marine, *High Speed Solutions for Harbor and Terminal Tugboats* (Caterpillar Marine, Hamburg, 2014).

44. EIT InnoEnergy, *Unlocking New Possibilities Through Innovative Energy Storage: The Role of Ultracapacitors in the Energy Transition* (InnoEnergy—Frost&Sullivan, Eindhoven, The Netherlands, 2020).

45. D. Göhlich, T.-A. Fay, and S. Park, "Conceptual Design of Urban E-Bus Systems With Special Focus on Battery Technology," in *Proceedings of the Design Society: International Conference on Engineering Design* (2019).

46. Corvus Energy, "Corvus Orca ESS datasheet," 05 09 2023.: https://corvusenergy.com/products/energy-storage-solutions/corvus-orca-energy/ [Accessed 31 10 2024].

47. E-Mobitech, *High Power Series HP 7 Battery: Technical Datasheet* (E-Mobitech, Kocaeli, Turkey, 2022).